# The Possibility for Improving Damage Tolerance of Integral Airframe Structure by High Strength Bonded Straps

Vaclav Jetela, Josef Klement, Petr Augustin
Faculty of Mechanical Engineering, Brno University of Technology. Technicka 2896/2, 616 69 Brno. Czech Republic.
E-mail: vaclav.jetela@vutbr.cz, klement@fme.vutbr.cz, augustin@fme.vutbr.cz

**Integral stringer panels can attain weight reduction in primary aircraft structures, but do not contain the physical barriers for a fatigue crack growth. One of the promising techniques for prolonging a fatigue crack growth is bonded crack retarders made of materials with high stiffness. An experimental study was done on two specimens with different geometries. High strength bonded straps made of corrosion resistant steel AISI 301 were adhesively bonded to Center-Cracked Tension (CCT) specimens made of aluminium alloy 2024-T351 and fabricated by a high-speed machining process to promote fatigue crack growth retardation. Specimens were tested at a constant amplitude load. The study concludes that the fatigue crack growth life can be significantly improved. Experimental results were compared with a prediction based on the VCCT technique and the NASGRO equation.**

**Keywords:** Bonded crack retarder, Damage tolerance, Fatigue crack growth, Integral structure, Strap

## 1 Introduction

Aircraft structure failure can lead to catastrophic scenarios, where not only an aircraft but also human lifes might be tragically harmed. Integrally stiffened structures preserve minimum section size in highly loaded applications. This main advantage leads to the weight reduction in aircraft structure [1]. Unfortunately, integral structures have poor crack growth properties. The fatigue crack growth (FCG) in the proximity of stiffener will not be delayed compared to a built-up structure. The crack propagates directly into the stiffener [2].

First, mechanisms and general requirements for crack retarders are examined; this is followed by a description of specimen preparation and fatigue crack growth testing. Then, a detailed insight into the numerical analysis is mentioned. This paper will therefore discuss the potential of high-strength bonded straps as an additional safety element in terms of damage tolerance increase.

## 2 Main findings of previous studies

The crack retarder's capability to slow crack propagation has been investigated with regards to various material combinations. Aluminium alloys 2024 and 7075 were usually used as a material for M(T) or SEN(T) specimens, while crack retarders were consisted of materials with better or at least equal mechanical properties.

In 1989 Schijve [3] concluded that bonded crack retarders (BCRs) are much more effective than riveted retarders. In terms of low fatigue sensitivity, high ultimate strength and low specific density, he suggested ARALL retarders as the most effective solution. Following study of Li and Zhang [4] based on numerical calculations showed that BCRs made of carbon/epoxy are more effective in transferring the load from the base material than Ti-alloy retarders. Two comprehensive studies were done by Boscolo et al. [5] and Irving et al [6]. In the first study, authors did many experiments with BCRs made of carbon/epoxy, glass/epoxy, GLARE, and Ti-alloy. They also developed a new modeling technique comprising a disbond behavior. The influence of size, material choice and location of BCR were investigated with respect to the FCG. In their study, important BCR design parameters were identified as the elastic modulus, cross-sectional area, location, and adhesive toughness. The second study was focused on the BCRs made of GLARE, Ti-alloy, Al-alloy, and carbon/epoxy. The GLARE and Ti-alloy BCRs were the most effective in the FCG retardation during the constant amplitude loading up to 60 MPa. However, only the GLARE maintained its consistent effectiveness across the variable amplitude loading. In addition, an extensive parametric analysis was also done by Molinari et al. [7]. They developed an analytical tool named LEAF to predict damage tolerance properties of the stiffened structure. It was concluded that the BCR with higher width to thickness ratio are more effective in the retardation.

These studies mainly focused on BCRs made of materials with high specific strength, high specific modulus, and low specific density. However, the potential of BCRs made of high-strength steel has not been studied. Despite its much higher specific density, the elastic modulus and tensile strength can both be 1.6x higher compared to Ti-6-4 alloy. Therefore, in this study, work-hardened high-strength corrosion resistant steel AISI 301 was chosen as a material for BCRs.

## 3 Mechanisms and requirements

*Secondary bending:* Due to the unsymmetrical configuration of the panel stiffened with BCRs, the secondary bending will occur. The secondary bending has the negative consequence on the FCG [8].

*Disbonding:* When the crack passes under the BCR, a progressive disbond starts at a bonded interface. The straps can still carry the load but are less effective because of the lack of shear transfer capability [4]. The disbonding effect promotes a negative contribution to the FCG. This effect can be influenced by using a high strength adhesive or advisable surface pretreatment methods [9]. The BCRs made of cross-ply laminates are recommended for the weaker adhesives, because a complete disbond can be retarded. For the tougher adhesives, the best stacking sequence is the unidirectional layup provided that under the

load spectrum the strap does not disbond completely [6]. The disbonding can also be triggered by the cyclic loading of bonded structure resulting in a fatigue degradation of an adhesive joint [10] [11].

*Stiffening:* Two parts made of dissimilar materials are bonded together and loaded by a tension. The same displacement should be maintained. The part made of material with the higher elastic modulus (e.g. BCR) transfer more load than the part made of material with the lower elastic modulus. Consequently, the BCR transfer load from the substrate. However, the BCR made of material with the higher elastic modulus could promote a disbond failure [12].

*Bridging:* The BCRs restrain the crack tip opening by restraining forces, the reduction of stress intensity factor is obtained [12]. The restraining forces depends on the strip stiffness between the edges of the delaminated area of the BCR [3]. The bridging has a favorable effect to the FCG.

*Thermal residual stresses:* When the coefficients of thermal expansion between the BCR and the substrate deviates, thermal residual stresses (TRS) will occur. The level of thermal residual stress is related to an environment temperature. In order to maintain the self-equilibrium in the structure, residual stresses act together [13]. A tensile TRS induced in a sheet is balanced by a compressive TRS induced in a stiffening element. The compressive TRS can negatively affect the FCG [14].

*Fatigue sensitivity:* When the crack is passing under the BCR, the crack nucleation can occur in an adjacent BCR made of fatigue sensitive material. The crack nucleation can promote BCR failure in the future, resulting in the shorter FCG life. This behavior was observed in the experiments where sheet and BCR were made of the same material, the Al-alloy [3].

## 4 Specimen description

The CCT specimens were high-speed milled from the sheet made of 2024-T351 aluminium (see Fig. 1 for dimensions). Tests were carried out on the CCT specimen with three different geometries. First, the referential (bare) Specimen 1 without grooves and bonded crack retarders (BCRs) were tested. The capability of retarding the crack growth was examined for Specimen 2 with one steel layer and Specimen 3 with two steel layers (see Fig. 2 for BCR cross sections). The steel has high density, therefore, the material at the location of BCR (Specimen 2, 3) was removed; a potential weight increase in the CCT specimens was partly compensated. Mechanical properties and chemical compositions of substrate, BCR and adhesive are shown in Tab. 1, 2.

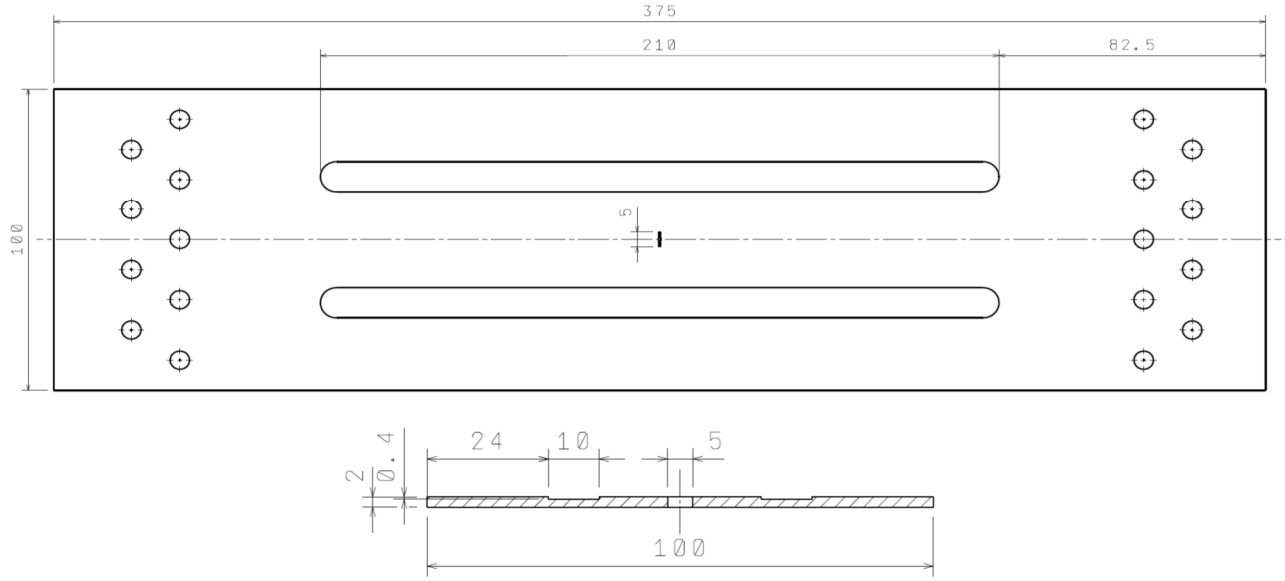


***Fig. 1*** *CCT specimen shape. The BCRs were bonded to grooves with the length 210 mm and the depth 0.4 mm. Dimensions in mm, not in scale.*

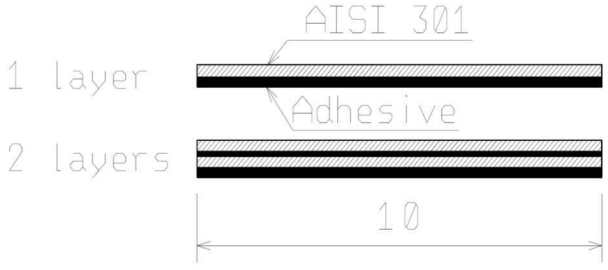


***Fig. 2*** *Bonded crack retarder cross sections. Dimension in mm, not in scale.*

Substrate surface pretreatment: The surface was degreased with acetone and FPL etched in the bath composed of 6.4 % $Na_2Cr_2O_7*2H_2O$, 23.4 % $H_2SO_4$ and 70.2 % $H_2O$ (weight fraction). The FPL etching duration was four hours at the ambient temperature. Finally, the substrate surface was rinsed in a water and blow-dried with the 45 °C air.

Strap surface pretreatment: Straps used for BCRs adhesive bonding were cut out of the sheet made of 0.255 mm thick AISI 301 corrosion resistant steel and degreased with acetone. After that, the straps were immersed in the solution containing 12.5 % HF, 40.8 %

$H_2O$, and 46.7 % $HNO_3$ for 20 minutes at ambient temperature. In the end, rinsing in the water and blow-drying with the 45 °C air took place.

Adhesive bonding: In case of Specimen 2 and 3, BCRs were bonded onto the specimen surface by the two-component Araldite® 2011 structural adhesive. Specimen 2 with BCR represented by one steel strap was cured for 24 hours at ambient temperature and for 30 minutes at 80 °C. In case of Specimen 3, first, two pretreated straps were bonded together and cured. An excessive adhesive layer on the outer surfaces was removed. Then, resulting BCRs were degreased with acetone and immersed in the solution containing $H_2O$, HF and $HNO_3$ for 20 minutes at ambient temperature. Finally, bonding onto the substrate and curing were done. The same curing process was used as in the case of Specimen 2.

***Tab. 1*** *Mechanical and thermal properties of substrate, bonded crack retarder and adhesive*

| | | | 2024-T351[a] | AISI 301 | Araldite® 2011 |
|---|---|---|---|---|---|
| Young's elastic modulus | E | [GPa] | 72.4 | 185[b] | 1.9[e] |
| Shear modulus | G | [GPa] | - | - | 0.9[e] |
| Poisson's ratio | ν | [-] | 0.33 | 0.27[c] | 0.52 |
| Thickness | t | [mm] | 2 | 0.255 | 0.2[f] / 0.2[g] / 0.1[h] |
| Density | ρ | [g/cm$^3$] | 2.77 | 8[d] | 1.05[e] |
| CTE (20°C) | α | [10$^{-6}$/K] | 23 | 17[d] | - |
| Ultimate Tensile Strength | Rm | [MPa] | 470 | 1635[b] | - |
| Yield Strength | $Rp_{0.2}$ | [MPa] | 325 | 1508[b] | - |
| Elongation | A | [%] | 20 | 2.1[b] | - |
| Shear Strength | τ | [MPa] | - | - | 15 - 18[i] |

***Tab. 2*** *Chemical composition of substrate and bonded crack retarder material*

| | Si | C | Fe | Cu | Mn | Mg | Cr | Ni | Zn |
|---|---|---|---|---|---|---|---|---|---|
| 2024-T351[a] | 0.5 | - | 0.5 | 3.8 - 4.9 | 0.3 - 0.9 | 1.2 - 1.8 | 0.1 | - | 0.25 |
| AISI 301[c] | 1 | 0.15 | - | - | 2 | - | 16.0 - 18.0 | 6.0 - 8.0 | - |

[a] ASM INTERNATIONAL HANDBOOK COMMITTEE. (1990). Properties and selection: Nonferrous alloys and special-purpose materials. pp. 1 – 1328. ASM International, Netherlands.

[b] DYMÁČEK, P., KLEMENT, J. (2011). Properties and manufacturing of steel-C/epoxy fiber-metal laminates. In: *Proceedings of the Fourth Seminar on Recent Research and Design Progress in Aeronautical Engineering and its Influence on Education: Part II*, pp. 47-52. Institute of Aeronautics and Applied Mechanics, Warsaw.

[c] Stainless Steel - Grade 301 (2001). AZo Materials. In: *Atlas Speciality Metals*, Australia

[d] ASM INTERNATIONAL HANDBOOK COMMITTEE. (1990). Properties and Selection: Irons, Steels, and High-Performance Alloys. pp. 1 - 1063. ASM International, Netherlands.

[e] Araldite® 2011 (AW106 + HW953U): Two component epoxy paste adhesive. (2004). pp. 1 – 4. Huntsman Advanced Materials, Cambridge.

[f] Specimen 2; thickness between strap and substrate

[g] Specimen 3; thickness between strap and substrate

[h] Specimen 3; thickness between steel layers

[i] Lap shear strength test: AISI 301 + 2024-T351

## 5 Fatigue crack growth test and results

The specimens were subjected to a crack propagation test with the following parameters: $\sigma_h$ = 60 MPa, R = 0.1 and f = 15 Hz. The crack length was periodically measured by a microscope with a metric scale on both sides of the specimen. The cyclic load was applied until the final failure of specimen. During the crack propagation test no crack initiation was observed in the BCRs. The BCRs broke (Specimen 2) or disbond (Specimen 3) shortly after the substrate failure. Crack lengths were plotted against the number of cycles, thus crack propagation curves were obtained for tested specimens (Fig. 4).

## 6 Numerical analysis

A numerical simulation was performed with the commercial software Abaqus using the VCCT technique. Simplified models consisted of 8-node linear brick elements (C3D8R) for the substrate and 8-node continuum shell elements (SC8R) for the adhesive and the strap were incorporated (see Fig. 3 for the used mesh). Due to a symmetry with respect to the YZ plane, only half of the specimen was modelled. Linear elastic models were utilized with properties mentioned in the Tab. 1.

The BCR was connected with the substrate using the surface-to-surface TIE constrain [15]. The same contact definition was also used between the surfaces of individual BCR layers. Accordingly, the progressive disbonding was not considered in this analysis. The substrate consisted of two separate parts, which were bonded together by the node-to-surface contact. Only a small relative motion between substrate parts was assumed, and thus a small sliding approach was used. This approach is also computationally less expensive [15]. The contact area was limited by a set of nodes representing the predefined crack surface.

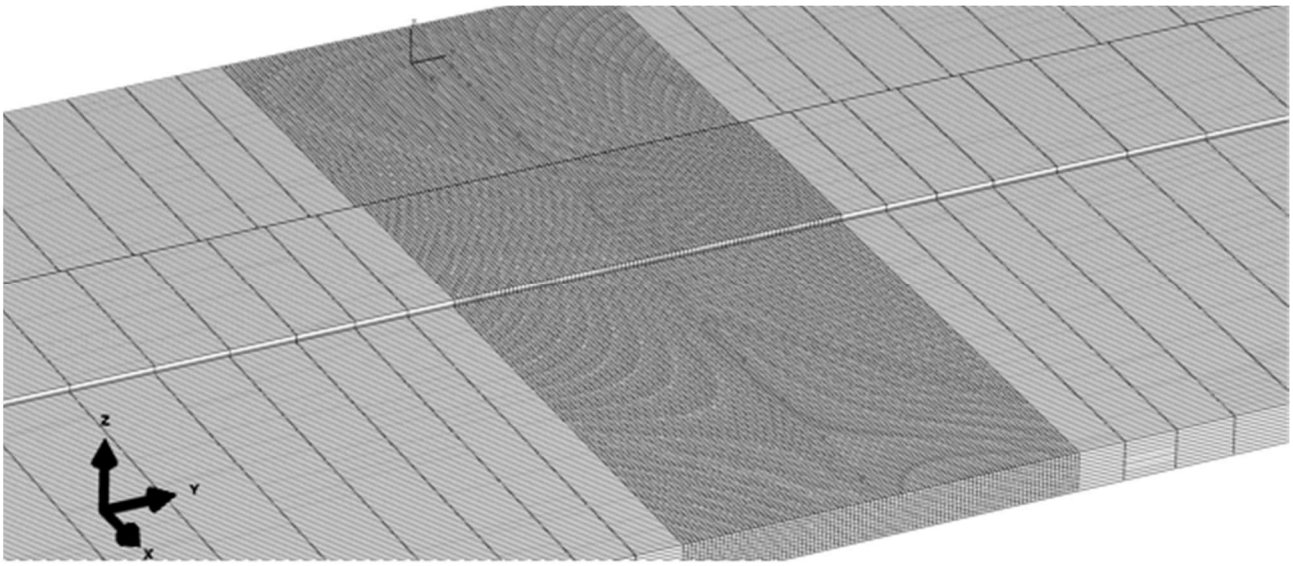


***Fig. 3*** *Overwiew of the mesh pattern along a predefined crack path for the 3D model (BCR: 2 x steel/adhesive layer)*

The strain energy release rate (SERR) was computed by the VCCT technique, which uses the principles of linear elastic fracture mechanics (LEFM). The VCCT is based on the assumption that the strain energy released when a crack is extended by a certain amount is the same as the energy required to close the crack by the same amount [15]. Three strain energy release rate components are calculated at a crack front node by

$$\boldsymbol{G = \frac{F \cdot \delta}{2A}} \tag{1}$$

where G is the column vector of strain energy release rate components, F consists of the forces at nodes along the crack front, δ is a row vector that consists of the relative displacements of the node pairs behind each corresponding crack front node, and A is the surface area created by crack growth [16].

The corresponding load was applied at the end of specimen in the Y direction; other remaining degrees of freedom were constrained. The opposing end was constrained in all directions (6 degrees of freedom). Due to the unsymmetrical configuration of specimen in the XY plane, secondary bending took place, and thus a non-linear analysis was performed. For each crack length, two analyses with different loads representing the upper and the lower level of the cyclic load were executed.

## 7 Fatigue crack growth prediction

First, resulting SERR values at each node of the crack front were averaged, thus the SERR for the upper level $G_{MAX}$ and the lower level $G_{MIN}$ were obtained. These averaged values were converted to stress intensity factors with the assumption of a plane stress conditions

$$\boldsymbol{K = \sqrt{GE}} \tag{2}$$

where G is the SERR, and E is the Young's elastic modulus of the substrate. Then the stress intensity factor range ΔK was given by

$$\boldsymbol{\Delta K = K_{MAX} - K_{MIN}} \tag{3}$$

A crack growth rate calculation was achieved by the NASGRO equation [18]

$$\boldsymbol{\frac{da}{dN} = C\left[\left(\frac{1-f}{1-R}\right)\Delta K\right]^{n} \frac{\left(1-\frac{\Delta K_{th}}{\Delta K}\right)^{p}}{\left(1-\frac{K_{MAX}}{K_c}\right)^{q}}} \tag{4}$$

where N is the number of applied fatigue cycles, a is the crack length, R is the stress ratio, ΔK is the stress intensity factor range, f is the crack opening function, $\Delta K_{th}$ is the threshold stress intensity factor, and C, n, p, and q are empirically derived constants. In this prediction, we used the curve fit of the NASGRO equation for the 2024-T351 Al-alloy (Data ID: M2EB11AB1) [19].

The incremental number of cycles ($\Delta N_i$) required for an incremental crack extension ($\Delta a_i$) at a crack length $a_i$ was then [13]

$$\boldsymbol{\Delta N_i = \frac{\Delta a_i}{(da/dN)_{a=a_i}}} \tag{5}$$

For each crack length, corresponding increments ($\Delta N_i$) were summed, thus predicted crack growth curves were obtained (see Fig. 4).

## 8 Results and discussion

The main purposes of this study were to investigate a potential FCG life increase by using high-strength BCRs and support these experimental results by numerical analyses. It was observed that BCRs made of AISI 301 high-strength steel can delay substrate failure. However, the crack growth prediction in the region behind the BCRs turned out to be partially problematic. Overall trends of FCG curves confirmed that damage tolerance of aircraft construction with AISI 301 steel BCRs could be increased.

With regards to experimental results (Fig. 4.), the FCG life of Specimen 2 increased by a factor of 1.4 and the FCG life of Specimen 3 substantially rose by a factor of 1.9. The BCRs led only to a slight weight increase of 4.7 % in Specimen 2 and 9.3 % in Specimen 3. For the bare specimen, the prediction was rather conservative with the difference of ≈ 4 % observed between crack lengths of 16–20 mm. The largest differences, 11 % (Specimen 2) and 14 % (Specimen 3), were recognized at the end of crack growth, although the prediction was still

conservative. In spite of the fact the region between 4.5 – 12 mm appears non-conservative. It is obvious that during propagation in real construction the additional secondary bending takes place as far the crack passes behind the stiffening element while the prediction is derived from pure tensile loading. This discrepancy could contribute to differences in the end of crack growth.

As previously mentioned, delamination was not considered during the numerical analyses. The prediction accuracy may be improved by incorporating the disbonding mechanism and thermal residual stresses (curing process). This research does not comprise the other possible positions and widths of BCR. The inclusion of these variables could lead to generalised conclusions. Nevertheless, their positive effect on FCG can be expected [5], [7]. Unfortunately, we were not able to measure the area of delamination, thus we cannot assess its impact on FCG. As mentioned in Main findings of previous studies, no one appears to have studied BCRs made of AISI 301 steel. Its great importance lies in high strength and elastic modulus which are one the most influential properties of BCR design resulting in less pricey safety inspections.

## 9 Conclusions

This study concludes that the FCG life of aircraft aluminium structure can almost be twice extended by BCRs made of two 0.255 mm thick layers of high-strength AISI 301 steel. It has been shown that utilizing the simplified analysis, the accuracy of predicted crack growth is reasonable up to the last edge of BCR. For a more precise prediction in the following region, the delamination behavior and residual stresses should be incorporated. Considering the improvement in FCG life, high-strength AISI 301 steel BCRs may be used in other dynamically loaded aluminium structures, e.g. marine structures.

The results of this paper will be compared to other possibilities promoting the FCG retardation. A study of the influence of crack retarders prepared by a cold spray technology and an autoclave technology on the FCG life is expected. The most promising technology will be applied onto the identical full-scale integral panel and the resulting increase in the FCG life will be compared to the bare integral panel, which was tested during the DaToN project [20].

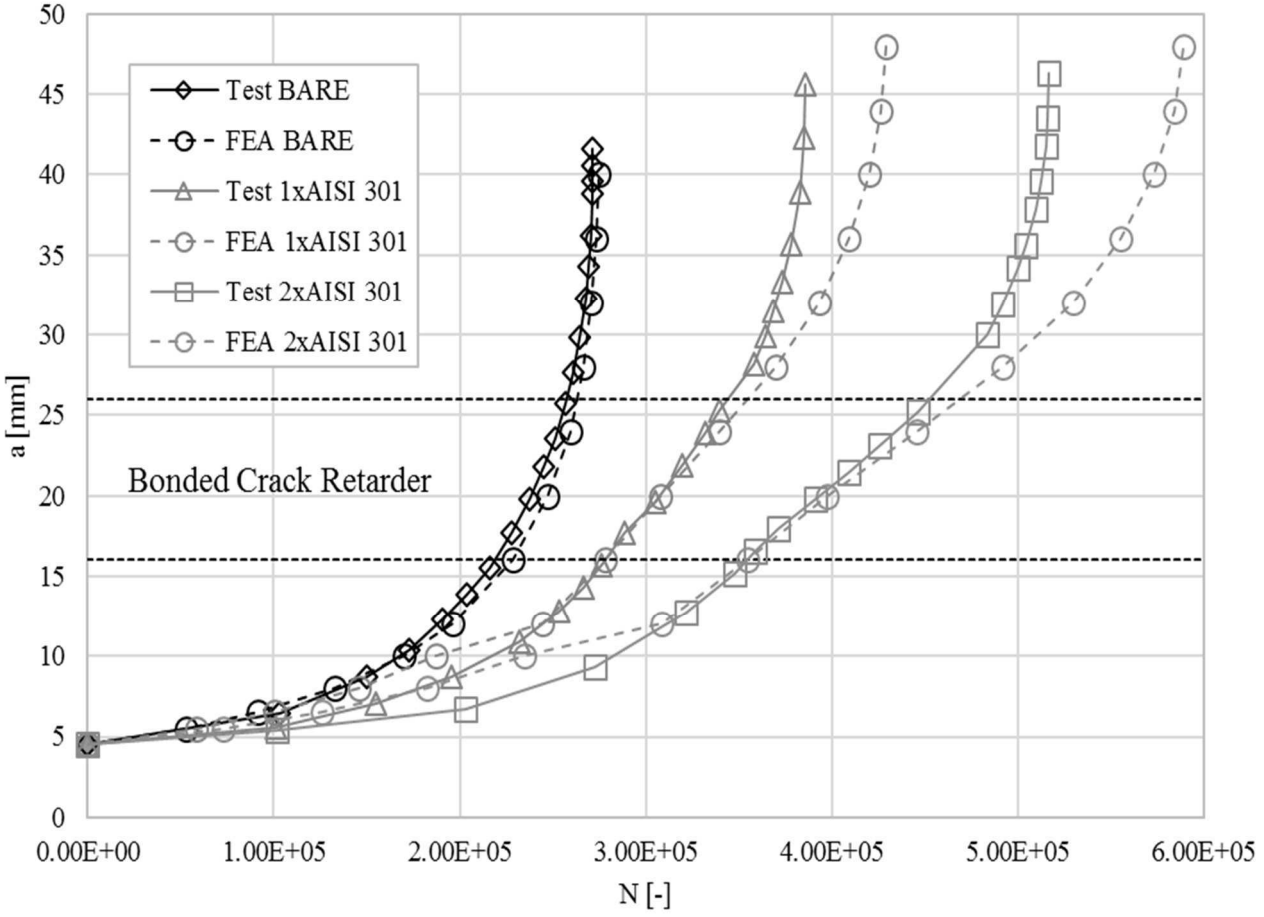


***Fig. 4*** *Crack propagation curves: CCT specimens with two different strap geometries*

## Acknowledgement

***The research leading to these results has received funding from the MEYS under the National Sustainability Programme I (Project LO1202).***

## References

[1] NIU, M. (1989). *Airframe structural design*, pp. 261. Conmilit Press Ltd., Hong Kong.

[2] NESTRENKO, G. (2000). *Comparison of damage tolerance of integrally stiffened and riveted structures*, pp. 6. ICAS Congress, Harrogate.

[3] SCHIJVE, J. (1990). Crack stoppers and arall laminates. In: *Engineering Fracture Mechanics*, Vol. 37, No. 2, pp. 405-421. Pergamon Press, New York.

[4] ZHANG, X., LI, Y. (2005). Damage Tolerance and Fail Safety of Welded Aircraft Wing Panels. In: *AIAA Journal*, Vol. 43, No. 7, pp. 1613 – 1623. American Institute of Aeronautics and Astronautics, Reston.

[5] BOSCOLO, M., ALLEGRI, G., ZHANG, X. (2008). Design and Modelling of Selective Reinforcements for Integral Aircraft Structures. In: *AIAA Journal*, Vol. 46, No. 9, pp. 2323 – 2331. American Institute of Aeronautics and Astronautics, Reston.

[6] IRVING, P., ZHANG, X., DOUCET, J., et al. (2011). Life Extension Techniques for Aircraft Structures – Extending Durability and Promoting Damage Tolerance through Bonded Crack Retarders. In: *ICAF 2011 Structural Integrity: Influence of Efficiency and Green Imperatives* (J. Komorowski, (Ed.)), pp. 753 – 770. Springer, Dordrecht.

[7] MOLINARI, G., MENEGHIN, I., MELEGA, M., TROIANI, E. (2012). Parametric damage tolerance design of metallic aeronautical stiffened panels. In: *The Aeronautical Journal*, Vol. 166, No. 1182, pp. 815-831. Royal Aeronautical Society, London.

[8] SCHIJVE, J., CAMPOLI, G., MONACO, A. (2009). Fatigue of structures and secondary bending in structural elements. In: *International Journal of Fatigue*, Vol. 31, No. 7, pp. 1111 – 1213, Elsevier, Netherlands.

[9] CIDLINA, J., MÜLLER, M. (2015). Influence of Adhesive Bonded Surface Treatment of Alloy Alcu4mg and Increased Environmental Temperature on Adhesive Bond Strength. In: *Manufacturing Technology*, Vol. 15, No. 4, pp. 520 – 526. Faculty of Production Technology and Management, Usti n. Labem.

[10] ŠLEGER, V., MÜLLER, M. (2015). Quasi static tests of adhesive bonds of alloy AlCu4M. In: *Manufacturing Technology*, Vol. 15, No. 4, pp. 694 – 698. Faculty of Production Technology and Management, Usti n. Labem.

[11] ŠLEGER, V., MÜLLER, M. (2016). Low-Cyclic Fatigue of Adhesive Bonds. In: *Manufacturing Technology*, Vol. 16, No. 5, pp. 1151 – 1157. Faculty of Production Technology and Management, Usti n. Labem.

[12] ZHANG, X., BOSCOLO, M., FIGUEROA-GORDON, D., et al. (2009). Fail-safe design of integral metallic aircraft structures reinforced by bonded crack retarders. In: *Engineering Fracture Mechanics*, Vol. 76, No. 1, pp. 114 – 133. Pergamon Press, New York.

[13] SCHIJVE, J. (2009). *Fatigue of Structures and Materials*, pp. 1 – 623. Springer, Netherlands.

[14] MENEGHIN, I., IVETIC, G., TROIANI, E. (2011). Analysis of Residual Stress Effect on Fatigue Crack Propagation in Bonded Aeronautical Stiffened Panels. In: *Material Science Forum*, Vol. 681, pp. 236 – 242. TTP. Switzerland.

[15] ABAQUS (2016). Abaqus 6.14 Documentation. Dassault Systèmes, Paris.

[16] ORIFICI, A., KRUEGER, R. (2010). Assessment of Static Delamination Propagation Capabilities in Commercial Finite Element Codes Using Benchmark Analysis. pp. 1 – 42. National Aeronautics and Space Administration, Hampton.

[17] NEWMAN, J. (1984). A Crack Opening Stress Equation for Fatigue Crack Growth In: *International Journal of Fracture*, Vol. 24, No. 3, pp. 131 – 135. Springer, Netherlands.

[18] NASGRO (2002). Nasgro Reference Manual 4.02. pp. 1 – 112. National Aeronautics and Space Administration Johnson Space Center, Houston.

[19] NASGRO (2002). NASMAT module. National Aeronautics and Space Administration Johnson Space Center, Houston.

[20] LANCIOTTI, A., LAZZERI, L., POLESE, C., et al. (2011). Fatigue crack growth in stiffened panels, integrally machined or welded (LBW or FSW): The DaToN project common testing program. In: *SDHM Structural Durability and Health Monitoring*, Vol. 7, No. 3, pp. 211 – 230. Tech Science Press, Duluth.

**10.21062/ujep/140.2018/a/1213-2489/MT/18/4/572**